UCRL-90681
PREPRINT

ESTIMATION OF THE THERMOPHYSICAL AND MECHANICAL PROPERTIES AND THE EQUATION OF STATE OF Li_2O

Oscar H. Krikorian

THIS PAPER WAS PREPARED FOR SUBMITTAL TO
THE PROCEEDINGS OF
9th European Conference on Thermophysical
Properties
Manchester, UK
September 17-21, 1984

September 6, 1984

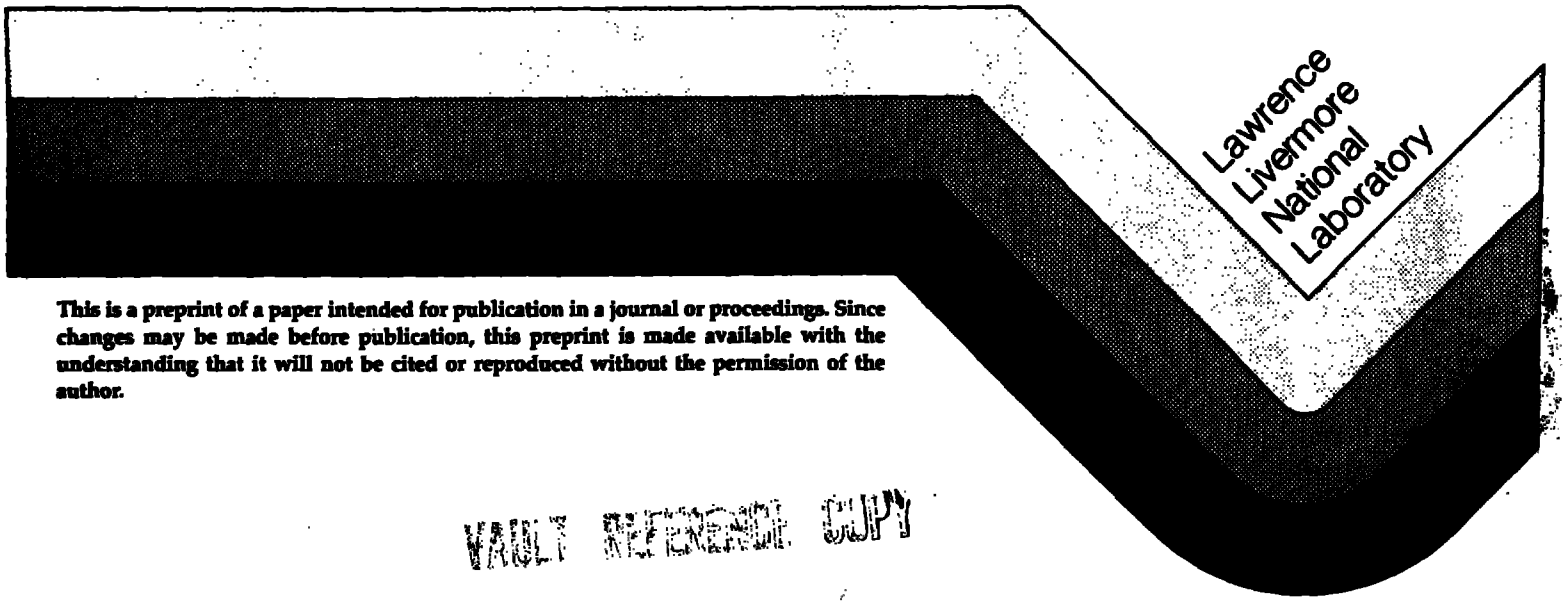

ESTIMATION OF THE THERMOPHYSICAL AND MECHANICAL PROPERTIES AND THE EQUATION OF STATE OF Li_2O*

Oscar H. Krikorian
Lawrence Livermore National Laboratory, P.O. Box 808, Livermore, CA 94550, USA
Presented at the EPTC 9th European Conference on Thermophysical Properties, UMIST, Manchester, UK, 17-21 September 1984

ABSTRACT. Lithium oxide is one the most important solid breeder materials for future use in magnetic or inertial-confinement fusion reactors. Yet, in spite of its potential use, very little experimental work has thus far been done on establishing the fabrication parameters and thermophysical and mechanical properties.

In this study we develop correlation methods based on Knoop microhardness and melting points for estimating tensile strength, Young's modulus, and Poisson's ratio for Li_2O as a function of grain size, porosity, and temperature. We also develop generalized expressions for extrapolating the existing data on thermal conductivity and thermal expansivity. Analytical expressions for these various properties are:

$$\sigma_t = 108\, d^{-0.4}\exp(-10p)(1 - 44\exp(-7000/T)),$$

$$E = 140\exp(-4p) - 140(T/T_m)\exp(-4p)\exp(1 - T_m/T),$$

$$\nu = 0.25,$$

$$k = (1 - p)^{1.94}(0.0220 + 1.784 \times 10^{-4}T)^{-1},$$

and $$\alpha = 2.0569 \times 10^{-6}T^{0.4},$$

where σ_t is tensile strength in MPa, E is Young's modulus in GPa, ν is Poisson's ratio, k is thermal conductivity in W/m-K, α is linear thermal expansivity in K^{-1}, d is grain diameter in μm, p is volume fraction porosity and T_m is the melting point of Li_2O in K.

Based on the available vapor pressure data on Li_2O and empirical correlations for the liquid and vapor equation of state of Li_2O, we also make estimates of the critical properties of Li_2O and obtain a critical temperature of approximately 6800 ± 800 K.

1 INTRODUCTION

Lithium oxide is one of the most important solid breeder materials for future use in magnetic or inertial-confinement fusion reactors because of its uniquely high lithium atom density coupled with a high melting point and relatively low volatility. The lithium atom density in Li_2O (~0.88 g Li/cm^3 at 1000 K) exceeds that in the pure metal by a factor of 2 and that in γ-$LiAlO_2$, the leading contender as a solid breeder, by a factor of 3. This high lithium atom density permits Li_2O to achieve a tritium breeding ratio of greater than one in a fusion reactor blanket without the use of neutron multipliers as required with other solid breeders.

*Work performed under the auspices of the U.S. Department of Energy by the Lawrence Livermore National Laboratory under contract number W-7405-ENG-48.

In pursuing the development of Li_2O as a solid breeder material, there is much yet to be done in establishing its fabrication characteristics, its compatibility with other materials, and its thermophysical and mechanical properties for design purposes. In spite of its potential use, surprisingly little is known about the above material characteristics of Li_2O.

It has been only recently that the thermal expansivity was measured by Kurasawa and coworkers (1982), the thermal conductivity was measured by Takahashi and Kikuchi (1980), and an accurate value for the melting point was determined by Ortman and Larsen (1982). Considerable work has been done on the vaporization characteristics ofLi_2O, and these studies have been summarized by Lamoreaux and Hildenbrand (1984). The microhardness of Li_2O has been reported by Nasu and coworkers (1978).

These data essentially comprise the available information on thermophysical and mechanical properties of Li_2O. We will therefore make estimates in ths paper of some of these unknown properties using mainly corelation methods. In addition to estimating properties of the solid we will also estimate the liquid-gas coexistance curve and the critical properties of Li_2O as a basis for better understanding its behavior in the liquid state.

2 ESTIMATION OF THE THERMOPHYSICAL AND MECHANICAL PROPERTIES OF LI_2O

Li_2O Microstructure

Very little is available in the literature on the microstructural characteristics of fabricated Li_2O specimens. Hence, the limited information reported by Takahashi and Kikuchi on specimens that they had fabricated for thermal diffusivity measurements is of considerable interest to us. They used the following fabrication procedure. Granules of the starting Li_2O material (designated as CERAC/PURE) were first heated in a platinum crucible under vacuum for four hours at 973 K to decompose LiOH and Li_2CO_3 impurities. The resultant material was then ground with an agate mortar and pestle in an argon atmosphere, pressed into pellets (10 mm diameter by 13 mm high) without a binder at 100-500 MPa, and sintered at temperatures of 1373 and 1473 K in covered platinum crucibles under vacuum for four hours. Specimens prepared in this way were sliced into discs 10 mm in diameter and 1.3 mm thick for the thermal diffusivity measurements. Total cation impurities were found to be 0.05 wt%, with Ca being the highest at 0.02 wt%.

Bulk densities for the specimens ranged from 70.8 to 93.4% of theoretical density (TD) with the average grain size ranging from 20 μm for 70.8% TD to 60 μm at 93.4% TD. Open porosity was found to be dominant at the lower densities, but as density increased the pores began to close off rapidly above about 86% TD. At 88% TD closed pores and open pores were found to be about equal, while above 90% TD closed pores dominated over open pores by about 5:1 (see Fig. 1).

An understanding of the pore structure variation with density is of value not only for interpreting physical and mechanical property behavior for Li_2O, but also for the insight it can give us on the mechanisms of tritium and helium release when Li_2O is used as a breeder. We should especially note that although Li_2O that has been sintered to temperatures as high as 1473 K and to a density of 93.4% TD, some 20% of the porosity still consists of open pores that should provide a network of passages throughout the structure for release of tritium and helium.

Thermal Conductivity

Using the methods of specimen preparation described above, Takahashi and Kikuchi (1980) measured thermal diffusivities of Li_2O in the range of 70.8 to 93.4% TD and temperatures of 473 to 1173 K. Thermal conductivities were then calculated from the thermal diffusivity values using literature information on specific heat and density to make the calculations. The data thus derived are summarized in Fig. 2, which also shows an extrapolation to 100% TD using the Maxwell-Eucken equation to make the extrapolation. We slightly modify the analytical expression used by Takahashi and Kikuchi to fit their data to express the thermal conductivity k in terms of volume fraction porosity p (instead of fraction of theoretical density) as follows:

$$k = (1 - p)^{1.94} (0.0220 + 1.784 \times 10^{-4} T)^{-1} \quad (1)$$

Thermal Expansivity

Kurasawa and coworkers (1982) have measured the percent thermal expansion up to ~1200 K for both single crystal and sintered specimens of Li_2O using a dilatometer to make the measurements. Two single crystal specimens, prepared from molten Li_2O by a floating zone technique, were used. Each specimen was 8 mm in diameter by 88 mm long. Five sintered specimens were prepared for the measurements using the method described by Takahashi and Kikuchi (see above). The sintered specimens were in the form of bars 4 x 4 x 10 mm, and had densities of 75.5, 80.0, 86.7, and 92.5% TD.

Kurasawa and coworkers' measurements on the single crystals showed a fair degree of variability between runs, especially at the higher temperatures. For example, the percent linear expansion from room temperature to 1173 K ranged from 2.47 to 2.82% for five different runs, which gives a spread of ± 6.6% about the mean. For each individual run, however, the standard deviation about a fitted curve for that run was quite good, being about 1-2%. Individual data points are not given for the sintered samples, but standard deviations are indicated to be of the order of 1% about the fitted curves. Agreement appears to be good for percent thermal expansion from room temperature up to about 1100 K for the averaged single crystal data and the sintered samples. Above 1100 K, the percent expansion curve shows a drop-off in slope with increasing temperature for samples with 80.0, 86.7, and 91.1% TD, but a normal continuation of the curves for 75.5, 92.5, and 100.0% TD.

In order to obtain thermal expansivity values from Kurasawa and coworkers' data, we need to differentiate the fractional expansion curves. We have a problem in doing this because of the variations in the data, especially at high temperatures. Therefore, our approach is to fit an average curve to the data up to 1100 K, and then allow the curve to rise in a predicted way above that temperature. The functional form of the curve is taken to be one that has previously been shown by Krikorian (1971) to be applicable to a large number of substances, including metals, oxides, borides, carbides, and nitrides, particularly at high temperatures. Thus, the averaged expression for fractional linear expansion, $\Delta L/L_0$ (where L_0 is referred to 298 K), and the expression for the derived linear thermal expansivity, α, are found to be as follows:

$$\Delta L/L_0 = - 4.275 \times 10^{-3} + 1.4692 \times 10^{-6} T^{1.4} \quad (2)$$

$$\alpha = d(\Delta L/L_0)/dT = 2.0569 \times 10^{-6}\, T^{0.4},\ K^{-1} \quad (3)$$

Fractional linear expansions calculated using equation (2) are compared in Table 1 with the average values for the single crystal data and for the 92.5% TD specimen as given by Kurasawa and coworkers. The linear thermal expansivity obtained from equation (3) is also summarized in Table 1.

Mechanical Properties

Experimental information on the mechanical properties of Li_2O is totally lacking at the present time. We must therefore rely on correlations based on other oxides to obtain some rough values with which to proceed with design calculations. Some theoretical guidance is also available in regard to variation of mechanical properties with grain size and specimen porosity. A primary design need for mechanical properties for Li_2O is to evaluate the thermal stress parameter, M, defined as follows:

$$M = \frac{\sigma_t\,(1 - \nu)k}{E\alpha},\ W/m, \quad (4)$$

where σ_t is the short term tensile strength, ν is Poisson's ratio, k is thermal conductivity, E is Young's modulus, and α is the linear thermal expansivity. We see that k and α are available for Li_2O as summarized earlier in this section. The problem remains to estimate values for the tensile strength, Young's modulus, and Poisson's ratio.

We consider first the estimation of tensile strength for Li_2O. The only property measurement that we are aware of that may be an indication of tensile strength is the microhardness of Li_2O which has recently been measured by Nasu and coworkers (1978). These workers prepared sintered discs of Li_2O, 10 mm in diameter and 3 mm thick, using isostatic hot pressing at 1323 K under 100 MPa pressure. The as-prepared specimens (grain size ~50 μm) gave a Vickers microhardness of 180 ± 8 kg/mm^2 using a 300 g load for 30s on a diamond indentor. The microhardness was found to increase upon irradiation of the Li_2O, saturating to a value of 230 ± 7 kg/mm^2 with neutron doses exceeding 5 x 10^{17} neutrons/cm^2. The microhardness returned to its original value after annealing at temperatures above 623 K. It is not unusual to experience an increase in microhardness (and strength) of ceramics upon exposure to radiation as these workers found for Li_2O.

In order to develop a correlation between microhardness and tensile strength, we need data on oxides that have been adequately characterized for grain size and porosity. Such data are very limited because not only have relatively few oxides been well-characterized, but because of the brittleness of ceramics, tensile strength is a difficult property to measure. Recognizing these difficulties, we have nonetheless used data on microhardness and tensile strength given by Samsonov (1973) and Shaffer (1964) to obtain a rough correlation (see Fig. 3). Knoop rather than Vickers microhardness is used since that is what is generally available. The two types of microhardness are usually about equal where comparisons have been made. Grain sizes for the oxides are about 30 μm, porosities about 3%, and tensile strengths refer to ultimate short-term tensile strengths for the examples shown in Fig. 3. These oxide materials are generally believed to be of high purity except for ZrO_2 which is CaO-stabilized. From Fig. 3, we predict a tensile strength of about

20.5 MPa for Li_2O having a 30 μm grain size and 3% porosity.

The variation of strengths of ceramics with grain size and porosity is expressed in a generalized form by the following empirical expression originally given by Knudsen and referenced by Conrad (1970) and Wachtman (1967):

$$\sigma = \sigma_0 \, d^{-n} \exp(-bp), \tag{5}$$

where σ is the strength, d is grain diameter, p is the volume fraction porosity, and σ_0, n, and b are empirical constants. The general form of this equation differs slightly from that obtained from theoretical approaches, but the empirical expression seems to correlate well with oxide ceramics that have been studied. The value of n is usually somewhat less than 0.5, and b is about 10 according to Conrad (1970) and Wachtman (1967). Thus, using the value of 20.5 MPa for the tensile strength of Li_2O at a grain size of 30 μm and a porosity of 3%, we obtain:

$$\sigma_t(Li_2O) = 108 \, d^{-0.4} \exp(-10p), \tag{6}$$

where d is expressed in μm. Based on this equation, the variation of $\sigma_t(Li_2O)$ with grain size and porosity is illustrated in Table 2. Thus we see that grain size should be maintained below ~5 μm and porosity below ~5% in order to optimize the strength of the ceramic body.

This initial estimate of the tensile strength of Li_2O is probably good to within a factor of 2-3 of the true value, and most likely on the low side for the following qualitative reason. Li_2O has a relatively high melting point for a material with such a low microhardness. The high melting point is indicative of high bond strengths in the crystal and consequently of a high tensile strength.

In line with the behavior of other ceramics we expect that the strength of Li_2O will not vary significantly with temperature up to about 55-60% of its melting temperature at which point the strength will begin to decrease. We therefore predict that this decrease in strength begins somewhere in the region of 1000 K. This behavior can be expressed approximately by the relationship

$$\sigma_t = \sigma_0 \, (1 - 44 \exp(-7000/T)). \tag{7}$$

We discuss next the estimation of Young's modulus for Li_2O . Wachtman (1967) and Conrad (1970) have reviewed the theory and general behavior of elastic moduli for ceramics. From their observations and data presented by Shaffer (1964) and Samsonov (1973), we conclude the following. We can make a rough estimate of Young's modulus for Li_2O by correlating values of Young's modulus with the melting point of oxides. Grain size has no significant effect on Young's modulus at temperatures below the onset of grain-boundary sliding (i.e., below ~0.55-0.60 of the absolute melting point). However, porosity has a major effect on the modulus, leading to a decrease in modulus with increasing porosity. The effect of temperature is to give a slow rate of decrease of Young's modulus with increasing temperature until grain-boundary sliding sets in, at which point the modulus decreases rapidly until the

melting point is reached. Elastic constants are very dependent on structure, so that the various generalized conclusions discussed above only apply if phase transitions do not occur over the temperature interval of interest. Li_2O meets this criterion.

In order to obtain the best possible estimate of Young's modulus, we apply the correlation of Young's modulus versus melting point to only the cubic oxides (Li_2O has a cubic inverse fluorite structure), and use the available data from Shaffer (1964) and Samsonov (1973) after extrapolating to zero porosity. Data on non-cubic oxides such as Al_2O_3 and BeO show a significant deviation from the correlation, thus emphasizing structural effects. The cubic oxide correlation is illustrated in Fig. 4, where data on several representative cubic metals obtained from Samsonov (1968) are also included to show that the generalized correlation between Young's modulus and melting point is expected to be approximately linear. For Li_2O with a melting point of 1711 K (Ortman and Larson, 1982), we predict from Fig. 4 a Young's modulus of about 140 GPa at room temperature and zero porosity.

To predict the variation of Young's modulus with the porosity of Li_2O, we use the empirical Spriggs expression given by Conrad (1970) and Wachtman (1967):

$$E = E_0 \exp(-bp), \tag{8}$$

where E_0 is the value of Young's modulus at zero porosity (i.e., 140 GPa), b is an empirical constant, and p is the fractional porosity. We find b values of 4.0 for Al_2O_3, 4.7 for MgO, and 3.4 for BeO from data given by Samsonov (1973), Shaffer (1964), Conrad (1970) and Wachtman (1967). We therefore take $b = 4.0$ for Li_2O as our best guess, and the Spriggs expression for Li_2O becomes:

$$E(Li_2O) = 140 \exp(-4.0\ p),\ \text{GPa} \tag{9}$$

According to Wachtman (1967), the temperature dependence of Young's modulus for many ceramics can be described by an empirical expression of the type:

$$E = E_0 - AT \exp(-B/T), \tag{10}$$

where E_0 is Young's modulus at absolute zero, and A and B are empirical constants for each material.

We find that we can put equation (10) into a more generalized form by assuming (1) that E goes to zero at the melting point for those ceramic materials that do not undergo phase transitions prior to melting, and (2) that the constant B is equal to the melting temperature. The expression thus becomes

$$E = E_0 - (T/T_m)\, E_0 \exp(1 - T_m/T), \tag{11}$$

where T_m is the melting point. Examining the available data for Al_2O_3, MgO, ThO_2, UO_2, and MgO and CaO stabilized forms of ZrO_2 as given by Samsonov (1973) and Shaffer (1964), we find that there is good agreement with this expression up to at least 1200 K, and in some cases up to 1800 K. BeO, which undergoes a phase transition near its melting point, shows agreement up

to ~1300 K, but the experimental data indicate rapid drop-off of E above this temperature. In Table 3, the experimental and calculated temperature dependences of Young's modulus are compared for several representative oxides. We find that the agreement is quite good, especially considering the substantial systematic errors that are usually present in experimental data of this type. Predicted values for Li_2O with zero porosity are summarized in the last column of Table 3.

Finally, we need to estimate Poisson's ratio for Li_2O. Poisson's ratio is also related to Young's modulus and the shear modulus as follows:

$$\nu = \frac{E}{2\mu} - 1 \qquad (12)$$

Poisson's ratio for most materials, including ceramics, generally is found to be between 0.15 and 0.4. To a first approximation, Poisson's ratio should be independent of specimen porosity and temperature since both Young's modulus and the shear modulus show nearly the same porosity and temperature dependence. There are minor differences, however, and we especially might expect an increase in ν at high temperatures when grain boundary sliding becomes important (e.g., see Fig. 5). Small amounts of chemical additives may also influence Poisson's ratio. For example ThO_2 that contains 0.5% CaO exhibits a Poisson's ratio of twice that of pure ThO_2 (see Fig. 5).

It is difficult to make an accurate estimate of Poisson's ratio for Li_2O. Wide variations are seen in the reported data for even conventional ceramic materials such as Al_2O_3 and MgO (see Fig. 5) as based on data given by Samsonov (1973), Shaffer (1964), and Soga and Anderson (1966). We therefore choose to take roughly a mean value, based on all materials, of $\nu = 0.25$ for Li_2O, and further assume that ν is independent of porosity, temperature, and chemical purity. The uncertainty in this value could be as much as a factor of two.

Thermal Stress Parameter

We are now in a position to calculate values of the thermal stress parameter M for Li_2O as defined in equation (4). Analytical expressions are summarized in Table 4 for each of the input parameters, together with estimates of the uncertainties. It is evident from Table 4 that the uncertainties in the mechanical properties (σ_t, E, and ν) are quite large and translate into an overall uncertainty of about an order of magnitude in the thermal stress parameter M. Clearly, accurate experimental data on the mechanical properties of Li_2O are needed if we are to calculate accurate values of this thermal stress parameter for reactor design purposes.

Even though the absolute value of the thermal stress parameter is not very accurate, it is still useful for us to know the dependence of M on grain size, porosity, and temperature in attempting to optimize use conditions for Li_2O in a blanket. The porosity and temperature dependence of M for Li_2O with a grain diameter of 10 μm is illustrated in Fig. 6. It is apparent from this figure that a relatively large gain can be made in thermal stress parameter by using low porosity materials, especially with porosities less than about 5%. Fig. 6 also shows that M drops off fairly rapidly with temperature initially, but levels off at temperatures above ~800 K.

As can be seen from Table 4, grain size (d) affects only the tensile strength, and this effect is translated directly to M as a $d^{-0.4}$

dependence. For illustration, using a 10 μm grain diameter as a unit reference value, we calculate the following factors for the dependence of M on grain size:

grain dia (μm)	2	5	10	20	50	100
factor for M	1.90	1.32	1.00	0.76	0.53	0.40

We see that maintaining a small grain size can greatly increase both tensile strength and the thermal stress parameter, e. g., an increase of a factor of 4 in σ_t and M is to be expected if the grain size is maintained at 2 μm instead of 50 μm. In a sense, what we have is an indirect temperature dependent effect, since higher operating temperatures lead to the development of larger grains. It is possible, however, in many ceramic materials to limit grain growth by the use of suitable chemical additives. Thus, this emphasizes the importance in future research on fabrication studies of Li_2O to develop materials with small and controlled grain sizes.

3 ESTIMATION OF THE LIQUID-GAS COEXISTANCE CURVE AND CRITICAL PROPERTIES of Li_2O

The Gas Phase Composition Above Liquid Li_2O

In analyzing the gas phase composition above liquid Li_2O, we assume that Li_2O is vaporizing under relatively neutral conditions, and is undergoing congruent vaporization. We refer to both the recent thermodynamic data compilation of Lamoreaux and Hildenbrand (1984) up to 3000 K, and the JANAF (1971) data up to 6000 K, to summarize in Table 5 the relative moles of gaseous species produced for each mole of liquid Li_2O vaporized at temperatures of 2000-6000 K. Also, summing over the various partial pressures, we obtain the total gas pressure at saturation, P_{sat}, in the last column of Table 5, by assuming ideal gas behavior.

We now approximate the temperature dependence of P_{sat} by using an equation having the form of the Clapeyron equation, i.e.,

$$\ln P_{sat} = A + B/T.$$

Plotting log P_{sat} versus 1/T, as shown in Fig. 7, we obtain a reasonably good fit, which is given by

$$\ln P_{sat}(atm) = 13.30 - 36{,}300/T. \qquad (13)$$

According to Reid and Sherwood (1966), this Clapeyron-type expression is usually not a bad approximation for expressing the dependence of pressure on temperature from the normal boiling point to the critical point, and we will therefore use it for purposes of interpolating or extrapolating Li_2O data.

Estimation of Liquid and Vapor Densities

As a first step in establishing liquid and vapor densities for the liquid-gas coexistance curve of Li_2O, we need to extimate the density of liquid Li_2O at its melting point of 1711 K. Using the room temperature lattice constant for Li_2O (A_0 = 0.4619 nm) given by Wyckoff and taking the volume expansion to be 3 times the linear expansion given by equation (2), we

obtain a molar volume of 16.85 cm^3/mole for the solid at the melting point, which gives a density of $\rho = 1.773$ g/cm^3.

In order to estimate the density of the liquid, we now examine the available information on volume change upon fusion of compounds with the fluorite structure as well as the alkali halides and the minimal information available on oxides (see Table 6). Thus, we see that the very approximate value of +15.4% that is available for the volume change upon fusion of Li_2O is higher than observed for other compounds with the fluorite structure. Yet, this may not be unreasonable, since upon examining the data on alkali halides, we find that the lithium halides show a higher $\Delta V_f/V_s$ value than the other alkali halides. The data on oxides shows a very broad range, and about all that we can conclude is that SiO_2 is unusual in its behavior and that the $\Delta V_f/V_s$ value for Li_2O should not be very different than for the other oxides. We therefore take $\Delta V_f/V_s$ for Li_2O to be 15.4 ± 5%, which reduces the uncertainty from that originally assigned (see footnote b in Table 6). Using this value of $\Delta V_f/V_s$, we now proceed to calculate $\Delta V_f = 2.60$ cm^3/mole, or $V_\ell = 19.45$ cm^3/mole and $\rho_\ell = 1.536$ g/cm^3 for liquid Li_2O at its melting point.

Having established a reference value for the density of liquid Li_2O at its melting point, we now proceed to estimate the change of density with temperature. We first apply a corresponding states expression for liquid density developed by Riedel and reported by Lewis and coworkers (1961) as

$$\rho_\ell/\rho_C = 1 + 0.85(1 - T_r) + (1 - T_r)^{1/3}(1.89 + 0.91/\omega), \qquad (14)$$

where ρ_ℓ and ρ_C are the liquid and critical densities, T_r is the reduced temperature, and ω is the accentric factor used by Riedel as a measure of the departure of the intermolecular potential function from that of simple spherical molecules. If we let $T_r = 0$ in equation (14), as indicated by Riedel, we obtain a hypothetical density ratio at absolute zero of $\rho_0/\rho_C = 3.74 + 0.91\ \omega$. Dividing this into equatin (14), as we find that the resultant expression is insensitive to ω up to about $T_r = 0.8$, and the expression takes the form

$$\rho_\ell/\rho_0 = 0.2674 + 0.2273(1 - T_r) + 0.505(1 - T_r)^{1/3}. \qquad (15)$$

Now, anticipating that T_c will be somewhere in the vicinity of 7000 K, we find from equation (14) that $\rho_\ell/\rho_0 = 0.8991$ at 1711 K, and from our reference density value of 1.536 g/cm^3 at 1711 K, we obtain $\rho_0 = 1.708$ g/cm^3, which gives finally

$$\rho_\ell = 0.4568 + 0.3883(1 - T_r) + 0.863(1 - T_r)^{1/3}. \qquad (16)$$

Values of liquid density calculated from this expression up to ~0.8 of T_c are shown as solid squares in Fig. 8. We note also that using values of T_c of 6500 K or 7500 K in equation (16) does not significantly change the calculated values of ρ_ℓ plotted in Fig. 8.

We now take as an alternative approach for estimating ρ_ℓ, the hole theory for liquids as developed by Fürth (1941), and applied with good results by Bockris and Richards (1957) to the liquid alkali halides.

Hole theory assumes that a fraction θ of the liquid has essentially the same structure as the corresponding solid, and within the volume of this

solid-like structure are holes with a characteristic size which depends upon the surface tension of the fluid. The characteristic hole size, V_h, is given by Fürth as

$$v_h = (32/15\pi)(kT/\sigma)^{3/2}, \tag{17}$$

where k is the Boltzman constant and σ is the surface tension of the liquid. In order to calculate θ, Fürth compares the characteristic hole size with the size of a particle in the solid lattice and obtains solutions for three cases, namely: for hole sizes comparable to particle size θ = 0.37, and for hole sizes either much smaller or much larger than the particle size θ = 0.915.

Once θ is established, we can calculate the volume thermal expansivity, β, for the liquid using the relation

$$\beta = \beta_S\theta + \beta^*, \tag{18}$$

where β_S is the volume thermal expansivity of the solid extrapolated into the liquid region, and β^* is the contribution to the volume thermal expansivity by the holes. Assuming that the surface tension has the characteristic form

$$\sigma = a(1 - T_r)^b, \tag{19}$$

where a and b are parametric constants, and that the holes are single holes only (rather than associated), Fürth obtains the following expression for β^*,

$$\beta^* = \frac{v_h N_h}{V_\ell} \frac{(3/2)[T_c + T(b - 1)]}{T(T_c - T)}, \tag{20}$$

where N_h is the number of holes per mole, and b, according to Lewis and coworkers (1961), has the value 11/9. The factor $v_h N_h/V_\ell$ is most conveniently estimated from the volume change on fusion, i.e., $\Delta V_f/V_\ell$, which in our case is 2.60/19.45 = 0.1337. The extrapolated volume thermal expansivity of the solid, β_S, is taken as 3 times the linear thermal expansivity in equation (3), and hence

$$\beta_S = 6.171 \times 10^{-6} T^{0.4}. \tag{21}$$

Before proceeding with the hole theory calculation, we need to compare hole size, v_h, with the lattice particle size in Li_2O. To do this, we need an estimate of the surface tension of liquid Li_2O. Using a modified form of the Eötvös equation, we will assume for a given class of compounds that $\sigma V_a^{2/3}$ is proportional to enthalpy of vaporization at the boiling point, ΔH_v, where V_a is the volume per gram-atom and ΔH_v is also given on a gram-atom basis. Thus, comparing the available data on oxides (see Table 7), we find that the product $\sigma V_a^{2/3} \Delta H_v^{-1}$ remains reasonably constant with an average value of 5.72 dyne-cm/kJ at a temperature of ~2/3 of the boiling point. We therefore estimate the surface tension of liquid Li_2O to be 328 dynes/cm at 1711 K (see Table 7).

Using this surface tension value in equation (17), we obtain a characteristic hole volume of 1.3×10^{-23} cm^3 at the melting point of Li_2O. This can be compared with he size of the O^{-2} ion, which, assuming an ionic radius of ~0.14 nm, is 1.15×10^{-23} cm^3 at room temperature. The volume of Li^+ is about an order of magnitude smaller than this, and an Li_2O unit occupies on the average a volume of 3.2×10^{-23} cm^3 based on tne density of solid Li_2O. We will assume that it is the size of the O^{-2} ion that mainly defines the particle size for purposes of the hole theory, and since v_h is therefore comparable in size to O^{-2}, and we will take Fürth's value of 0.37 for θ.

Substituting equations (20 and (21) into equation (18) together with $v_h N_h / V_\ell = 0.1337$, $T_c = 7000$ K, $b = 11/9$, and $\theta = 0.37$, and then integrating equation (18), we obtain

$$V_\ell\ (Li_2O) = 19.45 \exp\ 0.8582 + 1.631 \times 10^{-6}\ T^{1.4} + 0.300 \ln T - 0.367 \ln (7000 - T)\ . \qquad (22)$$

We also note that substituting either $T_c = 6000$ K or 8000 K in equation (22) has little effect on the values of V_ℓ up to ~0.8 of T_c.

Using equation (22), we now calculate the values of ρ_ℓ for Li_2O based on hole theory as shown by the full triangles in Fig. 8. We see that the rate of density decrease with temperature is substantially greater based on hole theory than based on the Riedel equation. We believe that the hole theory densities are actually too low because of the assumption of a regular rate of decrease of σ with temperature (see equation (19)). It is actually found that many liquid oxides such as B_2O_3, SiO_2, GeO_2, PbO, and $LiBO_2$ (see Janz and coworkers, 1969) show an increase in σ with temperature (even though this trend must reverse as the critical point is approached). We also believe the Riedel equation densities are too high, simply because the rate of decrease of density with temperature is less than that in solid Li_2O. We conclude that the true values of ρ_ℓ lie somewhere between the hole theory and Riedel equation values.

We next proceed to sketch in the rectilinear diameters, D_R, based on both the hole theory and Riedel equation ρ_ℓ values, where D_R is given by

$$D_R = (\rho_\ell + \rho_g)/2, \qquad (23)$$

and ρ_g is the density of the gas, which for our purposes here is taken to be the ideal gas density derived from equation (13) by using an average molecular weight for the gas phase. We further sketch in a locus of critical densities by assuming a series of critical temperatures and correcting the ideal gas densities to that of a real gas at each assumed critical point using a critical compressibility factor of 0.291 as listed by Lewis and coworkers (1961) for an accentric factor of zero. We thus find (see Fig. 8) that the hole theory rectilinear diameter gives $T_c = 6400$ K, and the Riedel equation rectilinear diameter gives $T_c = 7350$ K. We select 6800 ± 800 K as our best estimate of T_c, and construct the coexistance curve as shown by the solid line in Fig. 8 to give a linear rectilinear diameter. The real gas densities used in constructing Fig. 8 are summarized in Table 8.

Summarizing the estimated critical properties of Li_2O from Table 8, we find a critical temperature of 6800 ± 800 K, a critical pressure of ~2,900 atm, a critical density of ~0.32 g/cm^3, and a critical volume of ~93 cm^3/mole.

REFERENCES

Bockris J O M, Richards N E, 1957 Proc. Roy. Soc. (London) A241 pp 44-66

Brewer L, Rosenblatt G M, 1969 in Advances in High Temperature Chemistry, Volume 2, Editor L Eyring (New York: Academic Press) pp 1-83

Conrad H, 1970 in Chemical and Mechanical Behvoior of Inorganic Materials, Editors A W Searcy, D V Ragone, U Columbo (New York: Interscience) pp 391-411

Drowart J, Colin R, Exsteen G, 1964 report WADD-TR-60-762, Part XXVI, Air Force Materials Laboratory, Research and Technology Division, Air Force Systems Command, Wright-Patterson Air Force Base, Ohio

Fink J K, Chasanov M G, Leibowitz L, 1981 J. Nucl. Mater. 102 pp 17-25

Fürth R, 1941 Proc. Cambridge Phil. Soc. 37 pp 252-275

JANAF Thermochemical Tables, second edition 1971, Project Directors D R Stull, H Prophet (Washington D.C.: U.S. National Bureau of Standards)

Janz G J, 1967 Molten Salts Handbook (New York: Academic Press) pp 39-51, 80-88, 93-95, 184, 248-264

Janz G J, Dampier F W, Lakshminarayanan G R, Lorenz P K, Tomkins R P T, 1968 Molten Salts: Volume 1, Electrical Conductance, Density, and Viscosity Data, Nat. Stand. Ref. Ser., Nat. Bur. Stand. (U.S.) NSRDS-NBS 15 (Washington D.C.: Superintendent of Documents, U.S. Government Printing Office) pp 1-139

Janz G J, Lakshminarayanan G R, Tomkins R P T, Wong J, 1969 Molten Salts: Volume 2 Section 2. Surface Tension Data, Nat. Stand. Ref. Data Ser., Nat. Bur. Stand. (U.S.) NSRDS-NBS 28 (Washington, D.C.: Superintendent of Documents, U.S. Government Printing Office) pp 49-111

Kirshenbaum A D, Cahill J A, 1960 J. Inorg. Nucl. Chem. 14 pp 283-287

Krikorian O H, 1971 report UCRL-51043, Lawrence Livermore National Laboratory, Livermore, California

Kurasawa T, Takahashi T, Noda K, Takeshita H, Nasu S, Watanabe H, 1982 J. Nucl. Mater. 107 pp 334-336

Lamoreaux R H, Hildenbrand D L, 1984 J. Phys. Chem. Ref. Data 13 pp 151-173

Lewis G N, Randall M, Pitzer K S, Brewer L, 1961 Thermodynamics (New York: McGraw-Hill) pp 605-629

Nasu S, Fukai K, Tanifuji T, 1978 J. Nucl. Mater. 78 pp 254-256

Ortman M S, Larsen E M, 1982 report UWFDM-449, Nuclear Engineering Department, University of Wisconsin, Madison, Wisconsin

Reid R C, Sherwood T K, 1966 The Properties of Gases and Liquids, second edition (New York: McGraw-Hill) pp 114-116

Samsonov G V, 1968 Handbook of the Physicochemical Properties of the Elements (New York: IFI Plenum) pp 387-394

Samsonov G V, 1973 The Oxide Handbook (New York: IFI/Plenum) pp 23-35, 235-245, 256-262

Shaffer P T B, 1964 Plenum Press Handbooks for High-Temperature Materials -- No. 1. Materials Index (New York: Plenum Press) pp 308-387

Skinner B J, 1966 in Handbook of Physical Constants, revised edition, Editor S P Clark, Jr (New York: The Geologic Society of America, Inc.) p 90

Soga N, Anderson, O L, 1966 J. Amer. Ceram. Soc. 49 pp 355-359

Takahashi T, Kikuchi T, 1980 J. Nucl. Mater. 91 pp 93-102

Touloukian Y S, Kirby R K, Taylor R E, Lee T Y R, 1977 Thermophysical Properties of Matter, Volume 13, Expansion Nonmetallic Solids (New York: IFI/Plenum)

Wachtman J B Jr, 1967 Ceramic Bulletin 46 pp 756-774

Wyckoff R W G, 1963 Crystal Structures, Volume 1, second edition (New York: Interscience)

Figure 1. The dependence of open and closed porosity in Li_2O as a function of overall specimen density is illustrated for Li_2O specimens fabricated by sintering.

Figure 2. Thermal conductivities of Li_2O are shown as a function of percentage of theoretical density and temperature according to the data of Takahashi and Kikuchi (1980).

Figure 3. A correlation of Knoop microhardness with tensile strength is illustrated for several oxide ceramics having an approximate grain size of 30 μm and a porosity of about 3%. For Li_2O with a reported Vickers microhardness of 180 kg/mm^2, this correlation predicts a tensile strength of 20.5 MPa.

Figure 4. The correlation of Young's modulus of elasticity with melting point is illustrated here for cubic oxides and metals. On the basis of this correlation, Young's modulus for Li_2O is predicted to be about 140 GPa.

Figure 5. Poisson's ratio is shown as a function of temperature for several oxides. The solid curves are from Samsonov (1973) and the dashed curves from Soga and Anderson (1966). The latter data are believed to be the more accurate and indicate that Poisson's ratio increases gradually with temperature and is relatively insensitive to porosity. Chemical additives, such as 0.5% CaO added to ThO_2, also can have an effect on Poisson's ratio.

Figure 6. Illustrated here are calculated values of the thermal stress factor M for Li_2O as a function of temperature and porosity at a fixed grain diameter size of 10 μm.

Figure 7. A plot is given here of the logarithm of gas pressure, P_{sat}, in equilibrium with liquid Li_2O as a function of inverse temperature.

Figure 8. Predicted coexistence curve for Li_2O liquid and gas.

Table 1. The fractional linear expansions for single crystal Li_2O and 92.5% TD sintered Li_2O reported by Kurasawa and coworkers (1980), are compared here with a best-fit equation to all of the Li_2O data. The linear thermal expansivity derived from the best-fit equation is also given.

T,K	$\Delta L/L_o$, single crystal	$\Delta L/L_o$, 92.5% TD	$\Delta L/L_o$, best-fit equation	$\alpha(K^{-1})$, best-fit equation
298	-0.00004	0.00006	0.00000	2.01×10^{-5}
400	0.00210	0.00196	0.00218	2.26×10^{-5}
500	0.00447	0.00408	0.00455	2.47×10^{-5}
600	0.00712	0.00642	0.00711	2.66×10^{-5}
700	0.01003	0.00901	0.00986	2.83×10^{-5}
800	0.01321	0.01184	0.01276	2.98×10^{-5}
900	0.01667	0.01491	0.01582	3.12×10^{-5}
1000	0.02040	0.01822	0.01901	3.26×10^{-5}
1100	0.02440	0.02176	0.02233	3.39×10^{-5}
1200	0.02867	0.02554	0.02578	3.51×10^{-5}
1300	0.03321	0.02957	0.02934	3.62×10^{-5}

Table 2. Predicted variation of the estimated tensile strength (MPa) of Li_2O with grain diameter and fractional porosity in a fabricated body.

Grain Diameter, μ	Fractional Porosity				
	0	0.05	0.10	0.20	0.30
1	108.0	65.5	39.7	14.6	5.4
5	56.7	34.4	20.9	7.7	2.8
10	43.0	26.1	15.8	5.8	2.1
50	22.6	13.7	8.3	3.1	1.1

Table 3. The observed variation of Young's modulus (in GPa) with increasing temperature is compared for several oxide ceramics with the behavior calculated using equation (11) and assuming the calculated values of Young's modulus to be identical to the observed values at room temperature. Equation (11) is used to predict the values for Li_2O in the last column. Sample porosities are given for the experimental data, and the melting points used in the calculations are also indicated.

	Al_2O_3 (p = 2%, T_m = 2320 K)		MgO (p = 2%, T_m = 2850 K)		ZrO_2 - 4% CaO (p = 4%, T_m = 3000 K)		ThO_2 (p = 3%, T_m = 3490 K)		Li_2O (p = 0%, T_m = 1850 K)
T,K	obs.	calc.	obs.	calc.	obs.	calc.	obs.	calc.	calc.
298	376	376	295	295	167	167	235	235	140
600	366	370	278	294	164	166	231	235	134
800	356	357	267	289	161	164	224	233	124
1000	344	333	257	279	155	159	216	229	108
1200	324	300	246	264	149	152	209	223	87
1400	294	258	234	244	122	142	200	214	63

Table 4. Analytical expressions for the estimated physical and mechanical properties of Li_2O are summarized here together with an assessment of the expected uncertainties.

Tensile strength (in MPa):

$$\sigma_t = 108\ d^{-0.4}\ \exp(-10p)\ (1 - 44\ \exp(-7000/T)),$$

where d = grain diameter in μm and p = volume fraction porosity.
Estimated uncertainty in σ_t is a factor of 2 to 3.

Young's modulus (in GPa):

$$E = 140\ \exp(-4p) - 140(T/T_m)\ \exp(-4p)\ \exp(1 - T_m/T),$$

where T_m is the melting point of Li_2O (1711 K).
Estimated uncertainty in E is a factor of 2 to 3.

Poisson's ratio:

$$\nu = 0.25$$

Estimated uncertainty in ν is a factor of 2.

Thermal conductivity (in W/m-K):

$$k = (1 - p)^{1.94}\ (0.0220 + 1.784 \times 10^{-4}\ T)^{-1}$$

Estimated uncertainty in k is about ± 5%.

Linear thermal expansivity (in K^{-1}):

$$\alpha = 2.0569 \times 10^{-6} T^{0.4}$$

Estimated uncertainty in α is about ± 7%.

Table 5. Listed here are the estimated equilibrium concentrations of gaseous species above congruently vaporizing liquid Li_2O. The total saturation gas pressure above liquid Li_2O based on these species is given the the last column.

		Moles of gaseous species produced for each mole of $Li_2O(l)$ vaporized[a]								
T,K	p_{Li_2O}, atm	$Li_2O(g)$	Li(g)	$O_2(g)$	LiO(g)	$Li_3O(g)$	$LiO_2(g)$	O(g)	$Li_2(g)$	p_{sat} atm
2000	5.4×10^{-3}	0.828	0.278	0.060	0.030	0.008	0.006	0.002	--	7.9×10^{-3}
2500	1.8×10^{-1}	0.754	0.334	0.064	0.074	0.024	0.006	0.008	--	3.0×10^{-1}
3000	1.7×10^{0}	0.646	0.414	0.070	0.132	0.050	0.006	0.020	--	3.5×10^{0}
3500	7.9×10^{0}	0.544	0.494	0.068	0.204	0.066	0.006	0.038	0.002	1.8×10^{1}
4000	2.1×10^{1}	0.464	0.530	0.056	0.282	0.080	0.006	0.050	0.004	6.7×10^{1}
5000	9.3×10^{1}	0.348	0.624	0.050	0.344	0.100	0.004	0.100	0.014	4.2×10^{2}
6000	2.4×10^{2}	0.298	0.612	0.046	0.366	0.110	0.002	0.116	0.028	1.3×10^{3}

[a] In addition to the neutral species listed at 6000 K, the gas also contains the following numbers of moles of charged species: 0.010 $Li^+(g)$, 0.006 $Li_3O^+(g)$, 0.008 $LiO^-(g)$, and 0.008 $e^-(g)$.

Table 6. Summary of values of the volume change on fusion relative to the volume of the solid at the melting point, $\Delta V_f/V_s$ (in %), for various halides and oxides.[a]

Fluorite structures		Alkali halides		Oxides	
Li_2O	~15.4[b]	LiF	29.4	PbO	15.6
CaF_2	9.5	LiCl	26.2	B_2O_3	9.0
SrF_2	7.6	LiBr	24.3	Al_2O_3	22.3
BaF_2	5.8	ave., all MX:	20.0	SiO_2	-7.6
$SrCl_2$	1.9	range, all MX:	10.0-29.4		
$BaCl_2$	-0.2				
UO_2	10.4				

[a] Liquid density data for the various halides, Li_2O, PbO, and B_2O_3 are from Janz (1967) and Janz and coworkers (1968), for UO_2 from Fink and coworkers (1981), for Al_2O_3 from Kirshenbaum and Cahill (1960), and for SiO_2 the data are those on SiO_2 glass given by Touloukian and coworkers (1977) with our extrapolation to the melting point. The solid density data for UO_2 are from Fink and coworkers (1981), for PbO and B_2O_3 are estimated, for SiO_2 from Skinner (1966), for Li_2O from equation (2), and the balance are from Touloukian and coworkers (1977) and Janz (1967) with extrapolations as needed.

[b] This value for the volume change on fusion of Li_2O is based on an estimated molar volume derived from data on silicate melts at 1673 K (Janz, 1967). The stated uncertainty of the estimate gives the range of $\Delta V_f/V_s$ values to be from 0.6-30.2%.

Table 7. This table illustrates the constancy of the surface tension parameter, $\sigma V_a^{2/3} \Delta H_v^{-1}$, for liquid oxides at ~2/3 of the boiling point.[a] The surface tension of liquid Li_2O at the melting point is calculated to be 328 dynes/cm based on the average value of 5.72 dyne-cm/kJ for the surface tension parameter of liquid oxides.

Liquid oxide	T,K	σ, dynes/cm	V_a, cm^3/g-atom	ΔH_v, kJ/g-atom	Est. B.P., K	$\sigma V_a^{2/3} \Delta H_v^{-1}$, dyne-cm/kJ
PbO	1223	133.4	13.89	131.4	1808	5.87
B_2O_3	1673	97.1	9.36	72.3	2338	5.96
Al_2O_3	2323	695	6.77	437.8	3800	5.68
SiO_2	2073	307.5	9.07	249.1	2800	5.37
Li_2O	1711	328 (calc.)	6.48	199.4	2730	5.72 (ave.)

[a] Data for σ are from Janz and coworkers (1969). Data for V_a are from Janz (1967) for PbO, from Janz and coworkers (1968) for B_2O_3, from Kirshenbaum and Cahill (1960) for Al_2O_3, from Touloukian and coworkers (1977) for SiO_2 as based on SiO_2 glass plus extrapolated data, and for Li_2O from this report. Data for ΔH_v have been derived from JANAF (1971) using the estimated boiling points given in this table.

Table 8. Summarized here for T_c = 6800 L for Li_2O are values of P_{sat}, average molecular weight, ideal gas density, and real gas density based on Z factors listed by Lewis and coworkers (1961).

T,K	P_{sat}, atm	ave. MW	ρ_g (ideal), g/cm^3	z	ρ_g (real), g/cm^3
2000	7.83×10^{-3}	24.86	1.19×10^{-6}	0.990	1.20×10^{-6}
2500	2.95×10^{-1}	23.64	3.40×10^{-5}	0.985	3.45×10^{-5}
3000	3.32×10^{0}	22.33	3.01×10^{-4}	0.975	3.09×10^{-4}
3500	1.87×10^{1}	21.01	1.37×10^{-3}	0.968	1.41×10^{-3}
4000	6.84×10^{1}	20.30	4.23×10^{-3}	0.951	4.45×10^{-3}
4500	1.87×10^{2}	19.53	9.91×10^{-3}	0.921	1.08×10^{-2}
5000	4.20×10^{2}	18.86	1.93×10^{-2}	0.868	2.25×10^{-2}
5500	8.12×10^{2}	18.68	3.36×10^{-2}	0.794	4.23×10^{-2}
6000	1.41×10^{3}	18.56	5.31×10^{-2}	0.696	7.63×10^{-2}
6500	2.24×10^{3}	18.39	7.73×10^{-2}	0.551	1.40×10^{-1}
6600	2.44×10^{3}	18.33	8.26×10^{-2}	0.508	1.63×10^{-1}
6700	2.65×10^{3}	18.27	8.81×10^{-2}	0.450	1.96×10^{-1}
6800	2.87×10^{3}	18.21	9.36×10^{-2}	0.291	3.22×10^{-1}

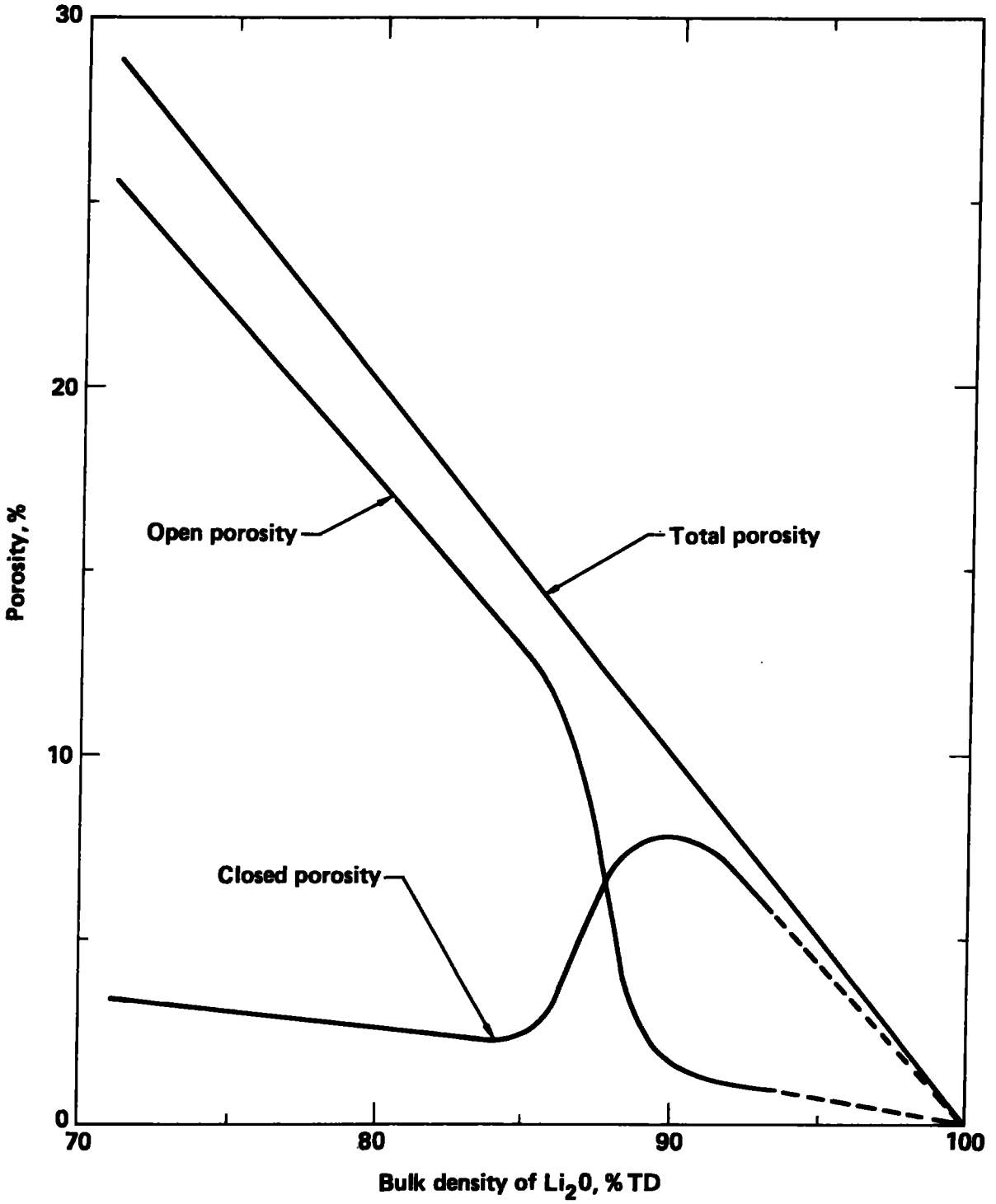

Figure 1. The dependence of open and closed porosity in Li_2O as a function of overall specimen density is illustrated for Li_2O specimens fabricated by sintering.

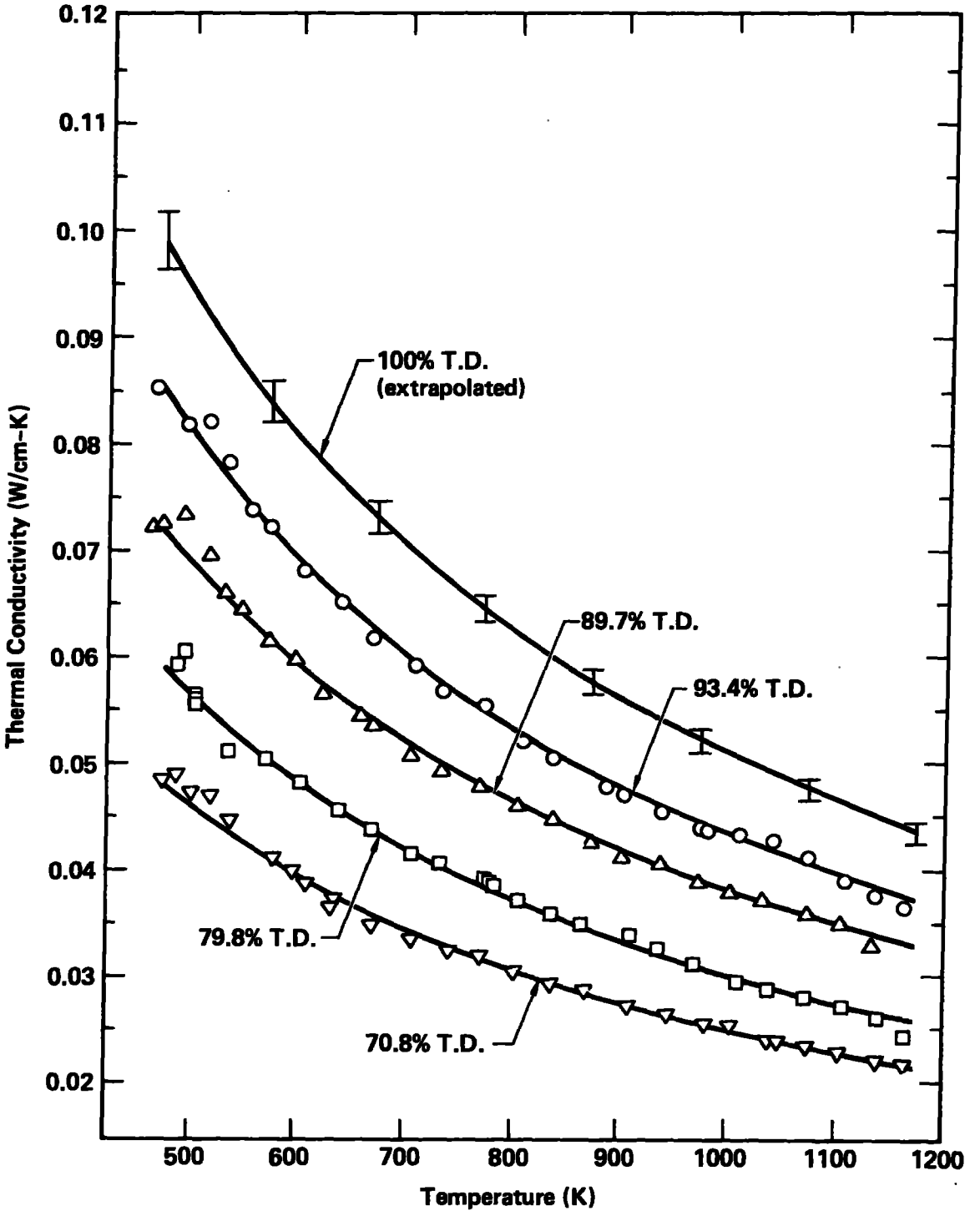

Figure 2. Thermal conductivities of Li_2O are shown as a function of percentage of theoretical density and temperature according to the data of Takahashi and Kikuchi (1980).

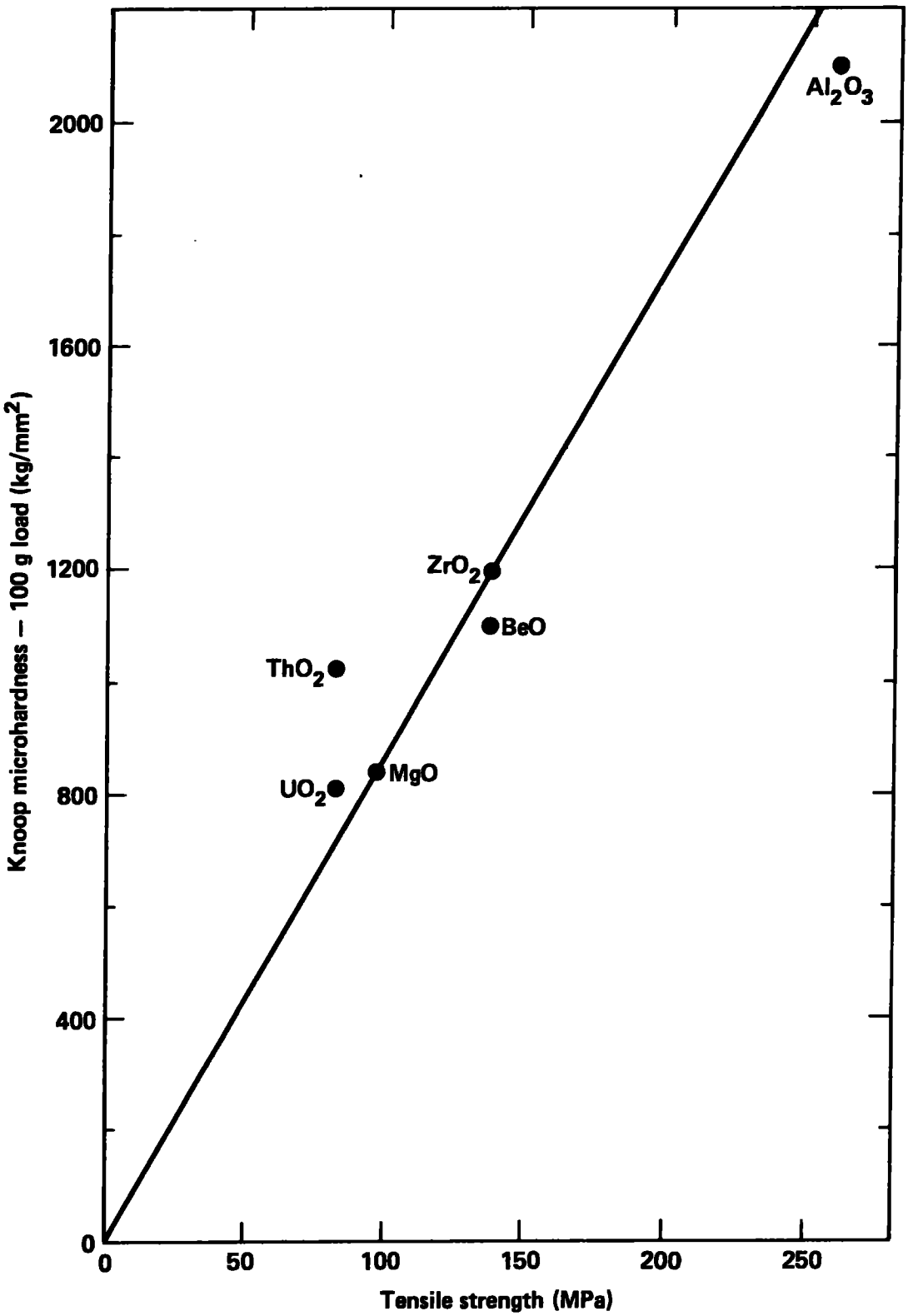

Figure 3. A correlation of Knoop microhardness with tensile strength is illustrated for several oxide ceramics having an approximate grain size of 30 μm and a porosity of about 3%. For Li_2O with a reported Vickers microhardness of 180 kg/mm², this correlation predicts a tensile strength of 20.5 MPa.

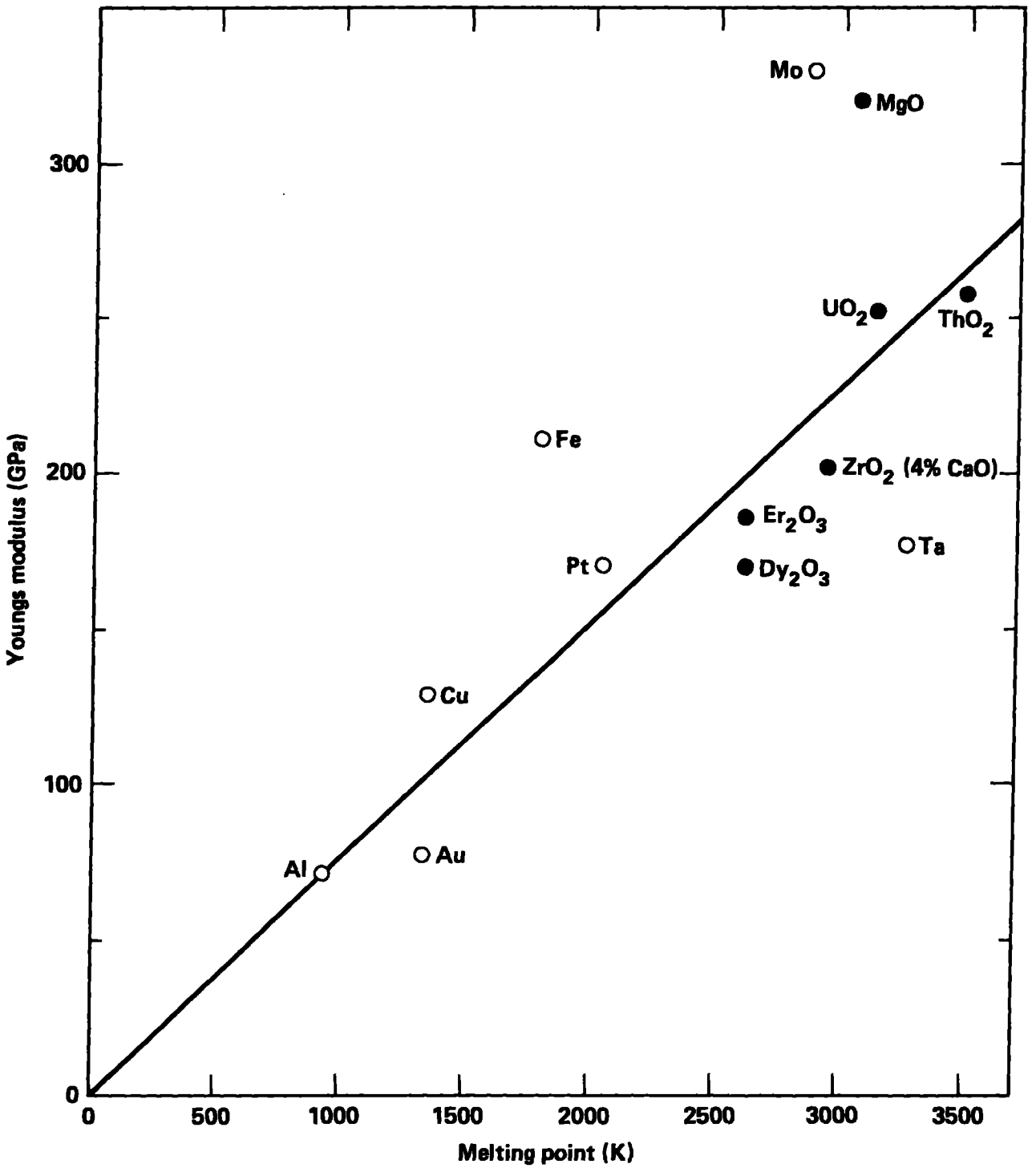

Figure 4. The correlation of Young's modulus of elasticity with melting point is illustrated here for cubic oxides and metals. On the basis of this correlation, Young's modulus for Li_2O is predicted to be about 140 GPa.

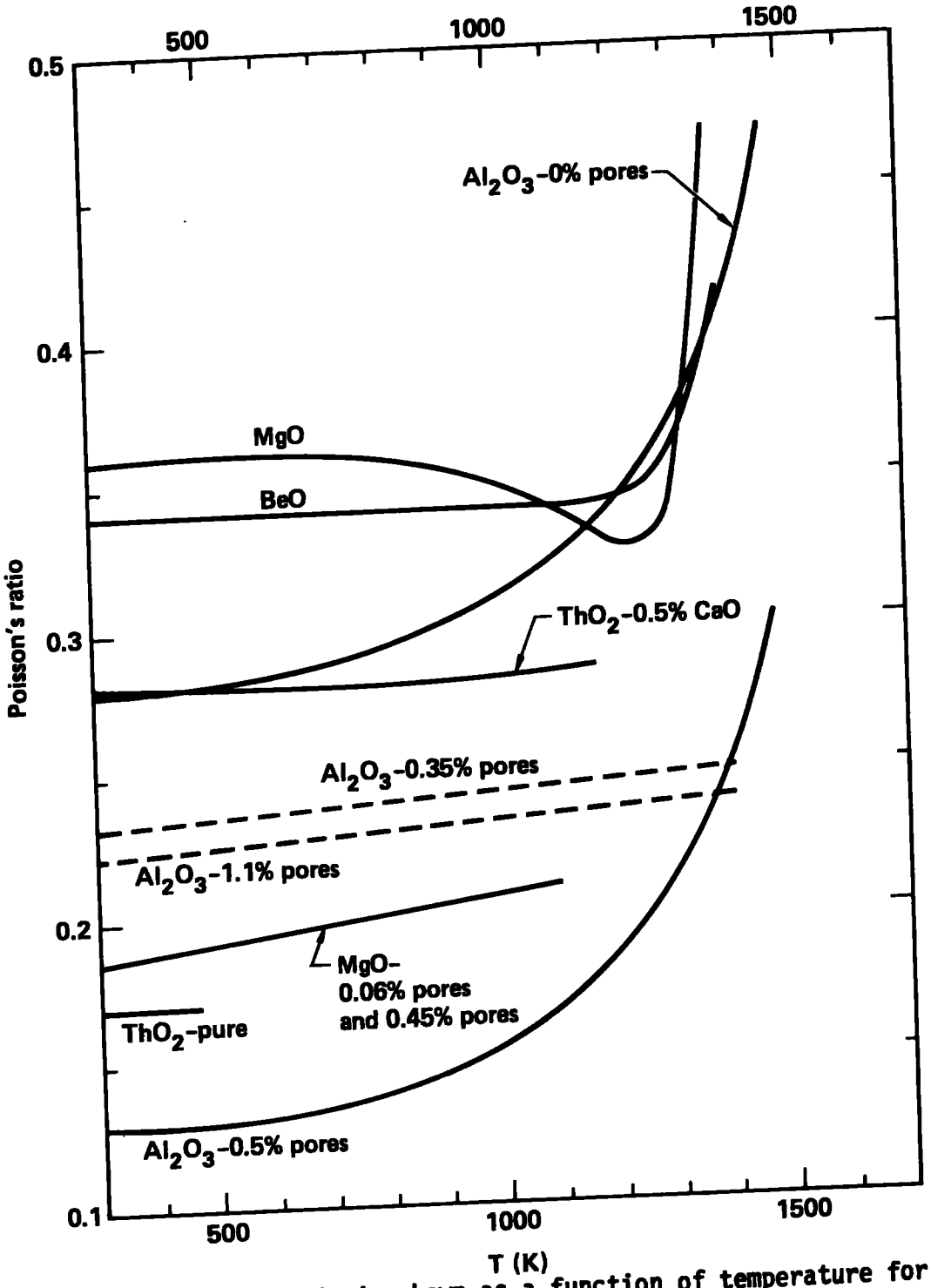

Figure 5. Poisson's ratio is shown as a function of temperature for several oxides. The solid curves are from Samsonov (1973) and the dashed curves from Soga and Anderson (1966). The latter data are believed to be the more accurate and indicate that Poisson's ratio increases gradually with temperature and is relatively insensitive to porosity. Chemical additives, such as 0.5% CaO added to ThO_2, also can have an effect on Poisson's ratio.

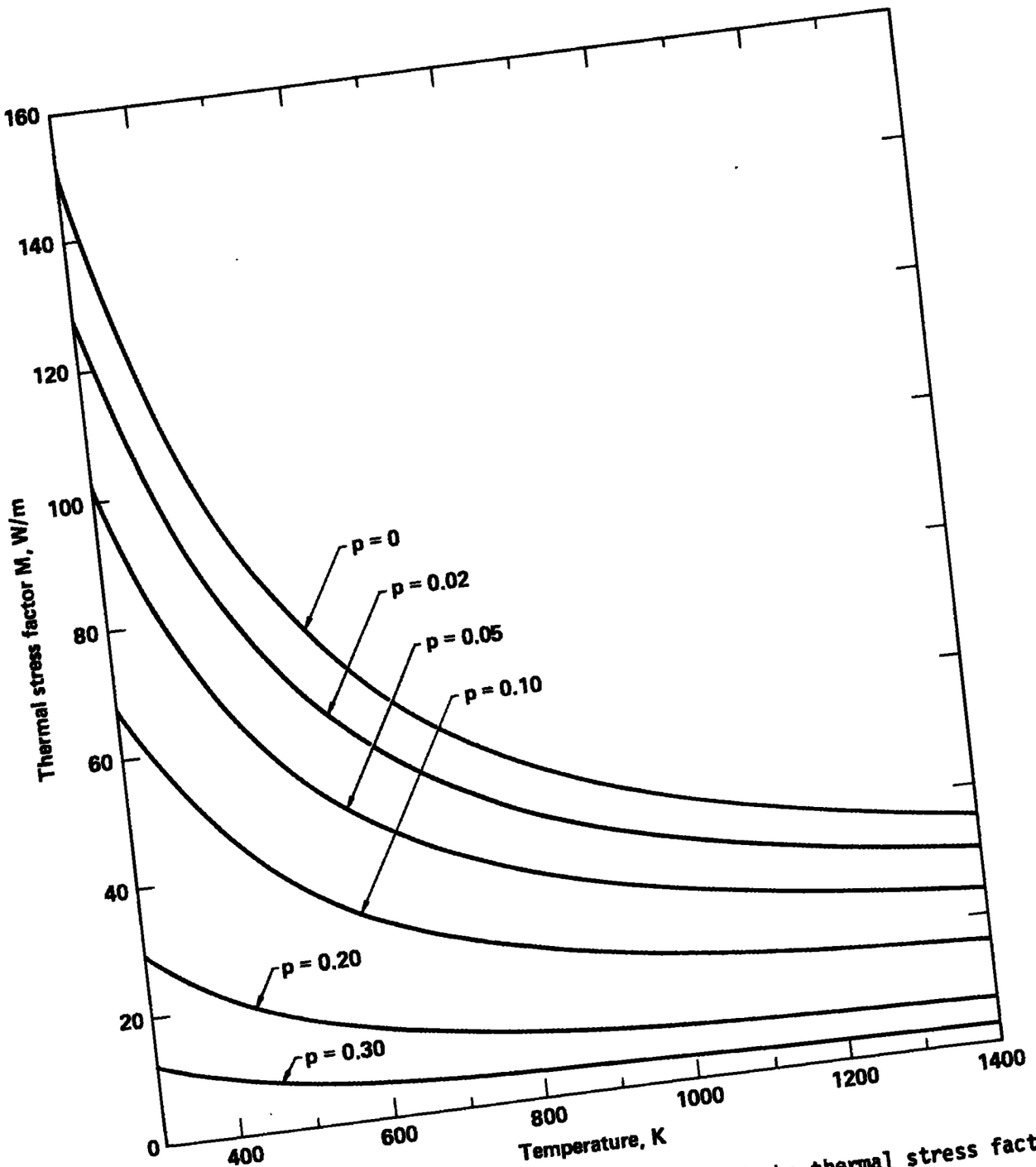

Figure 6. Illustrated here are calculated values of the thermal stress factor M for Li_2O as a function of temperature and porosity at a fixed grain diameter size of 10 μm.

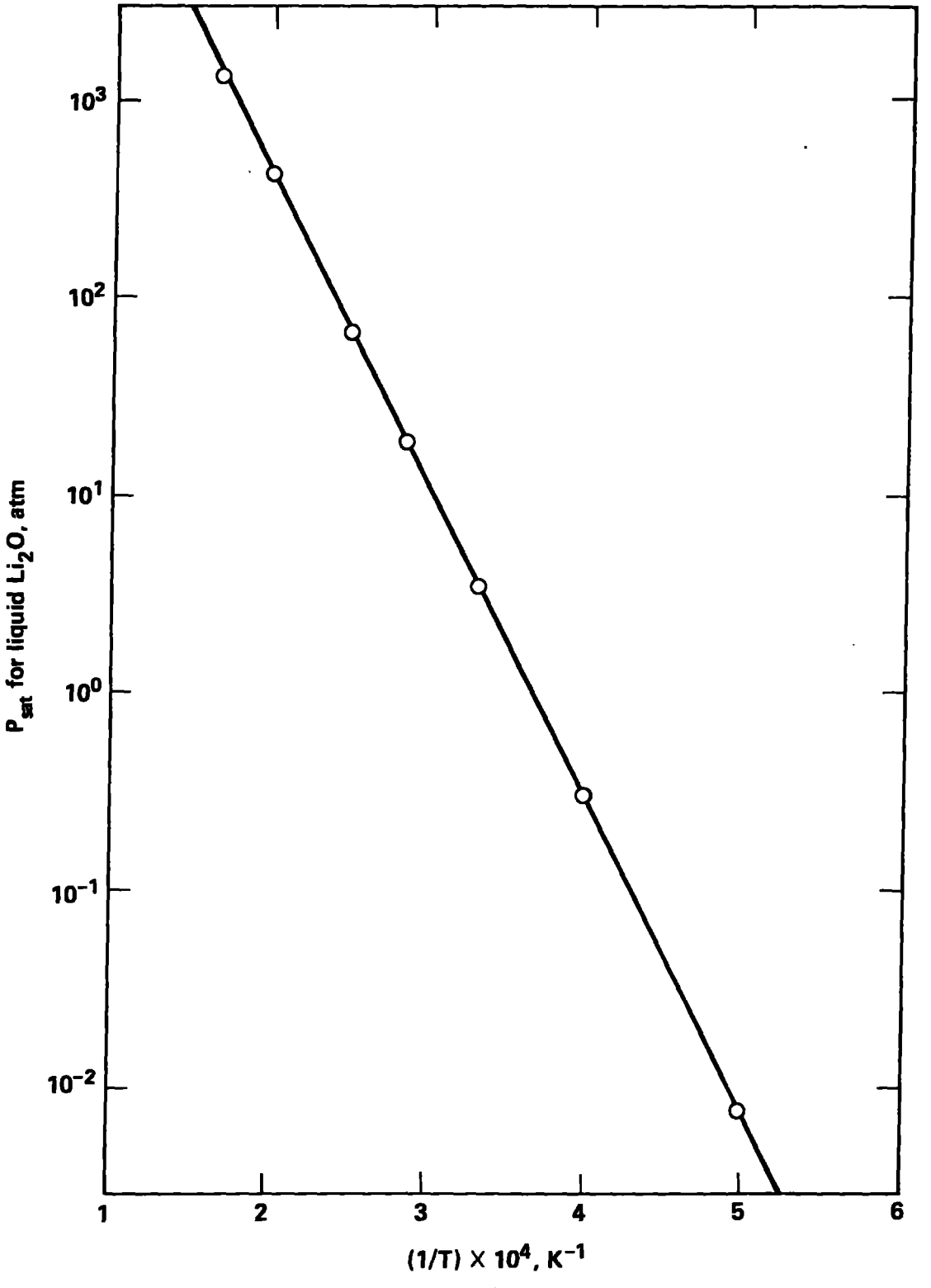

Figure 7. A plot is given here of the logarithm of gas pressure, P_{sat}, in equilibrium with liquid Li_2O as a function of inverse temperature.

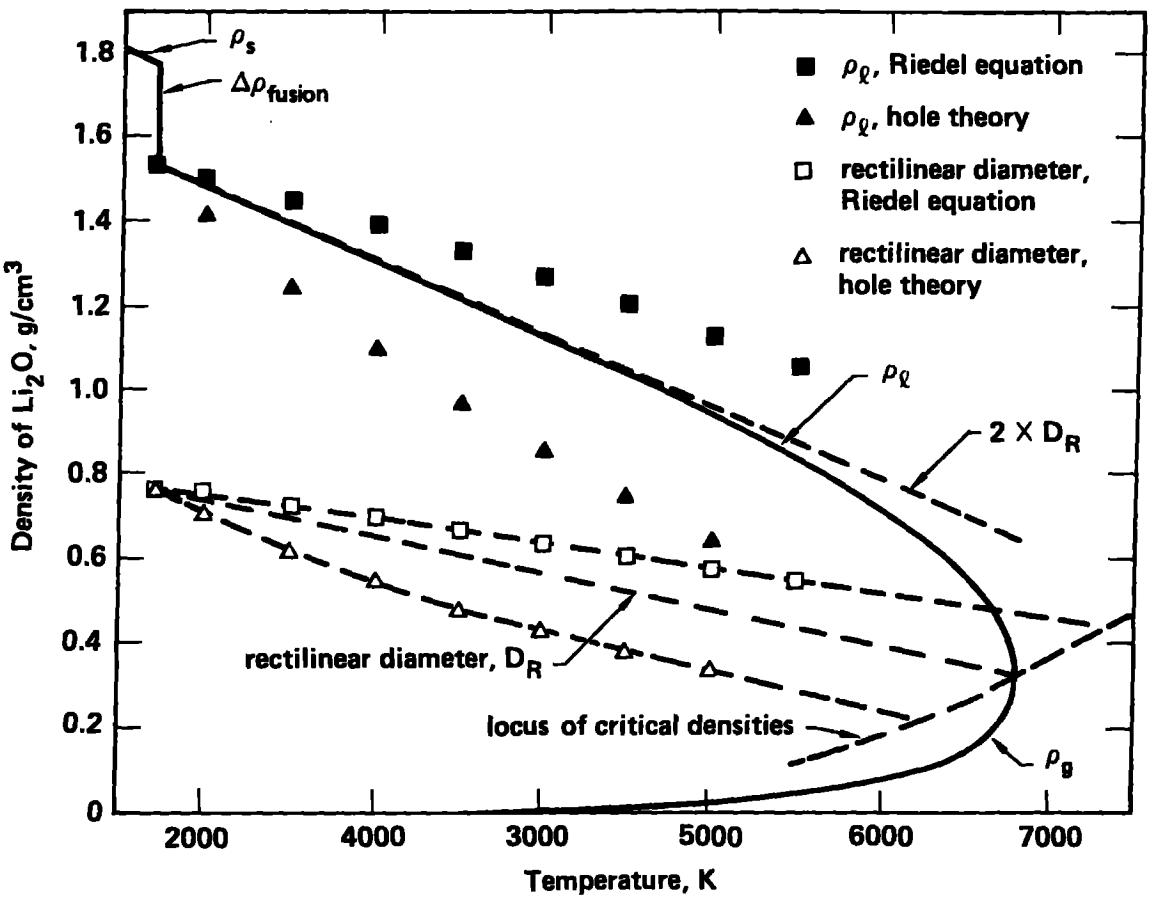

Figure 8. Predicted coexistence curve for Li_2O liquid and gas.